

SILICON MICROPLASMA DEVICES AS REAL-TIME SENSORS OF BULK PLASMA

BY

DONG SAN CHOI

THESIS

Submitted in partial fulfillment of the requirements
for the degree of Master of Science in Electrical and Computer Engineering
in the Graduate College of the
University of Illinois at Urbana-Champaign, 2014

Urbana, Illinois

Adviser:

Professor James Gary Eden

Abstract

Silicon microcavity devices have been demonstrated to exhibit photodetection capabilities. This thesis explores the possibility of using silicon microcavity devices as passive photodetectors for bulk plasma to serve as a diagnostic tool. The voltage-current characteristics of the device show that there is an interesting phenomenon that needs to be replicated with different types of devices to confirm what is occurring during operation. The discussion provides further insight on possible explanations for the voltage-current characteristics.

Acknowledgments

I would first like to thank my parents and my brother for their continual support in prayer and encouragement during this difficult season as a graduate student. I would also like to thank Eung Soo Kim, my predecessor, who taught me so much on microplasma research and silicon microcavity device fabrication. I need to express many thanks to all those who have helped me throughout my time at the Laboratory for Optical Physics and Engineering (LOPE). Special thanks to my advisers Professor J. Gary Eden, Professor Sung-Jin Park, and Professor Michael Loui who have been amazing role models. They believed in me and have provided the best opportunities for me to grow as a person and to grow in my career. Finally, I would like to thank my God, my Lord, for molding me to be the person He has called me to be.

Table of Contents

Chapter 1. Introduction.....	1
Chapter 2. Plasma Fundamentals.....	3
2.1 DC Plasma.....	3
2.2 Substituting n-type Material in a p-n Junction with a Plasma.....	5
Chapter 3. Experimental Methods.....	8
3.1 Device Fabrication.....	8
3.2 Experimental Setup.....	11
Chapter 4. Results and Discussion.....	17
Chapter 5. Limitations and Future Work.....	23
References.....	25

Chapter 1. Introduction

Plasma is considered to be the fourth state of matter. The other three are the more commonly known states: solid, liquid, and gas. Gas-phase plasma is formed by ionizing molecules or atoms through the application of heat or an electric field. It is comprised of electrons and positively or negatively charged ions and the bulk maintains overall neutrality. The observable universe is more than 99% in the plasma state. Microcavity plasma, or microplasma, refers to weakly-ionized, nonequilibrium gas-phase plasma that is confined to a cavity having a characteristic spatial dimension between 1 μm and 1 mm [1]. For weakly-ionized plasmas, less than 1% of the neutral gas is ionized and the temperatures associated with the electrons, ions, and neutral atoms are not the same. Microplasma devices have been fabricated in a variety of materials, including silicon, aluminum, glass, ceramic, and metal/polymer structures [2]. In 2002, photodetection in silicon microplasma devices was reported by Park et al. and further demonstrated by Ostrom in the following years [3]-[5]. A hybrid microplasma device having a silicon/plasma interface will be discussed as it pertains to the photodetection ability.

Because equipment using plasma-enhanced chemical vapor deposition (PECVD) and reactive ion etching (RIE) is commonly used in very-large-scale integration (VLSI), microelectromechanical systems (MEMS), and semiconductor fabrication techniques, a diagnostic tool assessing plasma uniformity would be ideal for monitoring the operation of these systems. Multiple photodetection devices could be placed inside the plasma chamber because microplasma devices are small in size. These photodetectors could provide real-time data concerning the plasma density (n_e) once a relationship was determined between plasma intensity and n_e . Further applications include mapping plasma intensity and density on a two-dimensional

or even three-dimensional scale depending on how many photodetectors are used and how they are placed within the chamber.

Chapter 2. Plasma Fundamentals

2.1 DC Plasma

The bulk of a plasma is quasi-neutral by having approximately equal electron and ion number densities (n_e and n_i , respectively). However, a charge imbalance can still occur within the plasma, and, in fact, is expected (for example) at a plasma-surface interface. The Debye length is the characteristic length scale in a plasma over which significant charge imbalance can occur.

The expression for the Debye length is:

$$\lambda_D = \left(\frac{\epsilon_0 T_e}{q n_e} \right)^{1/2} \approx 743 \left(\frac{T_e}{n_e} \right)^{1/2} (cm) \quad (1)$$

where ϵ_0 is the permittivity of free space, T_e is the electron temperature expressed in eV, q is the electron charge, and n_e is the electron density in cm^{-3} . Typical electron temperatures in microplasmas are 2-5 eV and the electron density is on the order of 10^{13} to 10^{16} cm^{-3} , thus resulting in Debye lengths on the order of 0.1-1 μm [6].

Although the bulk of the plasma is quasi-neutral, applying an external electric field accelerates the electrons very quickly along the field creating a charge separation along the field. The result is an ambipolar electric field that produces a restoring force and, in turn, reestablishes the quasi-neutral state of the plasma. The fundamental characteristic frequency of plasma results from this particle motion within the plasma, which is given by:

$$\omega_p = \left(\frac{n_e q^2}{m_e \epsilon_0} \right)^{1/2} \approx (5.65 \times 10^4) n_e^{1/2} (rad/s) \quad (2)$$

where m_e is the rest mass of the electron. Therefore, the typical plasma frequency ($f_p = \omega_p / 2\pi$) for microplasmas is on the order of 10-100 GHz .

When plasma is near the wall of its container, a positively charged sheath region will form and the quasi-neutrality characteristic of the plasma will no longer hold. Consider

an electrically grounded wall ($\Phi = 0$ V) that interacts with the plasma. Initially, the net charge density is zero at the boundary (due to the plasma's quasi-neutrality and $\rho = q(n_i - n_e)$) so there will be no potential or electric field. Then, some of the fast-moving electrons will be lost to the walls. But as the electrons are lost, the ion density increases near the wall. The accumulation of positive ions will begin to form the sheath. The net positive charge of the sheath will create a potential profile that is positive in the plasma but falls sharply to zero near the wall. Based on the potential profile, the resultant electric field will be directed from the edge of the bulk plasma to the wall. This electric field will direct electrons back into the plasma and keep ions within the sheath. Figure 1 illustrates these sheath phenomena:

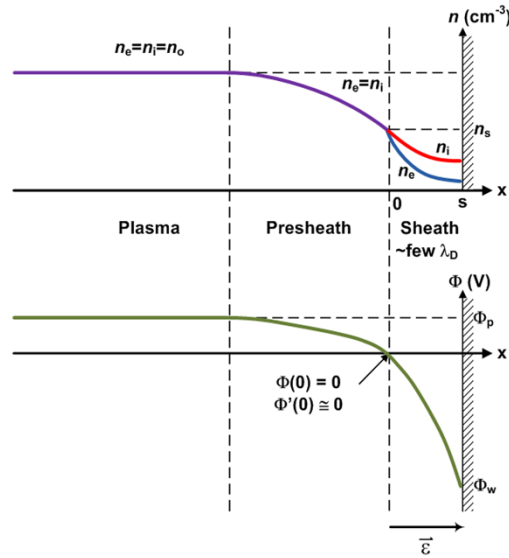


Figure 1. Charge density profile (top) and the potential profile (bottom) in the plasma, presheath, and sheath regions [7, 8].

There are models with which one can calculate the parameters of the sheath. One of the simplest examples is the matrix sheath which assumes two conditions. The first is that only ions are present in the sheath, and the second is that there is a uniform, constant, ion density within the sheath thickness [8]. If $n_i = n_s = \text{constant}$ and $n_e = \text{zero}$ at $x = 0$ (as it can

be imagined in Figure 1), the calculations will result in a linear variation in the electric field with a parabolic potential profile and sheath thickness, s :

$$E = \frac{en_s}{\epsilon_0} x \quad (3)$$

$$\Phi = -\frac{en_s}{\epsilon_0} \frac{x^2}{2} \quad (4)$$

$$s = \left(\frac{-2\epsilon_0\Phi_w}{en_s} \right)^{1/2} \quad (5)$$

2.2 Substituting n-type Material in a p-n Junction with a Plasma

The mathematical properties regarding charge transport in gas-phase plasmas and electron-hole plasmas of semiconductors have been recognized to be inherently the same [8], [9]. Plasma acts as a good conductor due to its high electron mobility even though the electron density is often lower than that for n-type silicon. The electron mobility in plasma is usually larger than the electron mobility in silicon [10]. The conductivity of plasma is given by the following (where $\mu_e \gg \mu_i$):

$$\sigma = q(\mu_e n_e + \mu_i n_i) \approx q\mu_e n_e \quad (6)$$

which is the same expression for n-type silicon. Not only are the current density equations the same, the equations regarding drift and diffusion currents are also the same. So using plasma in place of n-type silicon at the junction is within reason. Figure 2 is a good illustration of the comparison of the two types of junctions.

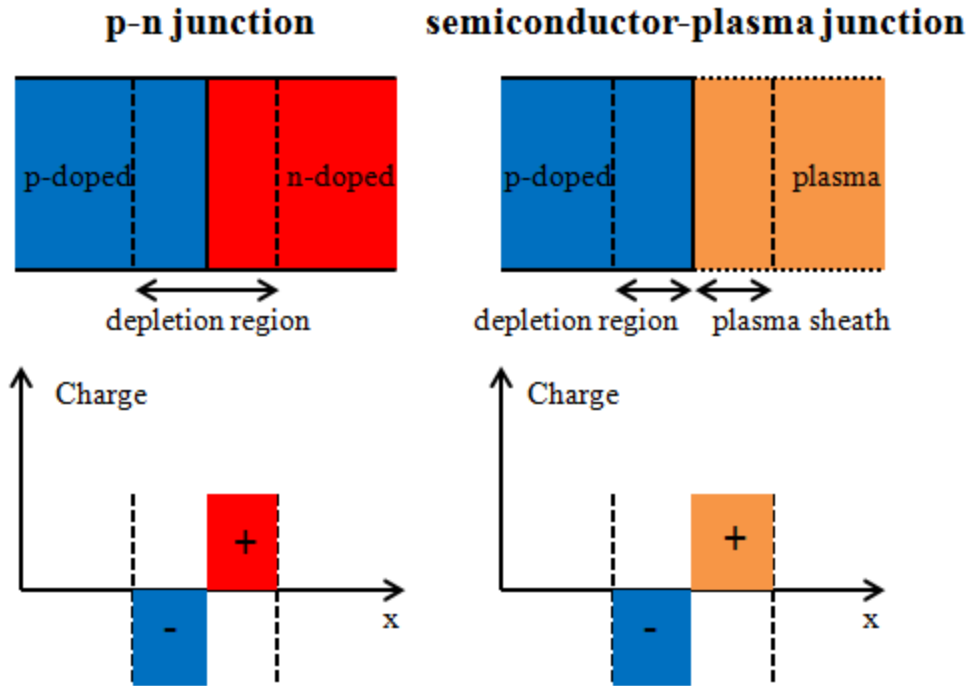


Figure 2. Comparison of a p-n junction and a semiconductor-plasma junction.

As illustrated in Figure 3, band bending occurs at the plasma interface in p-type silicon creating a depletion layer of majority carriers (holes) which results in a source of electrons near the interface. The tunneling barrier occurs due to the abrupt change in material from silicon to plasma. When voltage is applied and the plasma is ignited, the sheath distance (labeled as Cathode Fall in Figure 3) acts as a depletion layer which results in a high electric field that penetrates into the surface of the silicon, causing even more band bending.

When a photon is absorbed in the silicon near the depletion region, the electron will gain energy from internal electric field and penetrate the tunneling barrier assuming the voltage applied is high enough. This process is depicted for the silicon region in Figure 4. Once the electron is past the barrier and accelerated by the high electric field in the sheath, it is expected to undergo electron multiplication by avalanche. Avalanche occurs when an electron gains enough

energy between collisions from the high electric field to ionize the background gas through collisions, which in turn will produce more electrons that will also continue to ionize more gas.

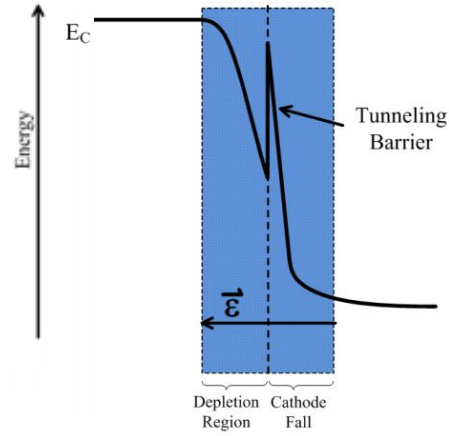


Figure 3. Qualitative energy band diagram for the junction between silicon and plasma. For clarity, only the spatial variation of the conduction band is shown (adapted from [7]).

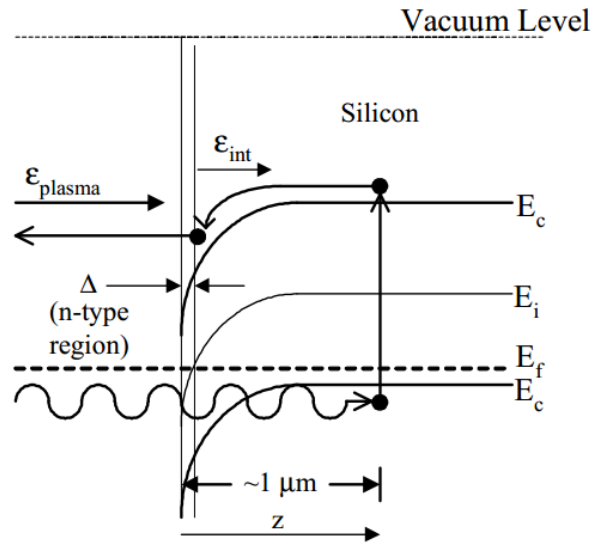


Figure 4. Qualitative band diagram for plasma/p-Si interface (adapted from [5]).

Chapter 3. Experimental Methods

3.1 Device Fabrication

The microcavity device is fabricated using techniques developed by VLSI and MEMS technology. A p-type <100> silicon wafer with boron doping of about 10^{15} - 10^{16} atoms/cm³ is used. First the wafer is placed in hydrofluoric acid diluted with water to remove the native oxide layer. A buffered oxide etchant can be used as well. Then a layer of silicon nitride (Si₃N₄) is deposited on both sides of the wafer using a Surface Technology Systems (STS) PECVD. Next, the surface is coated with a layer of AZ5214EIR photoresist (PR) to serve as a positive resist. Lithography is performed using the Karl Suss MJB-3 Mask Aligner to expose microcavity features of $50 \times 50 \mu\text{m}^2$. After developing the PR with AZ300MIF, the wafer undergoes RIE etching using the PlasmaLab Master Slave Dual-Chamber Reactive Ion Etcher (Slave side) with tetrafluoromethane (CF₄) as the etchant gas. The PR serves as a mask and silicon nitride is removed on the microcavity features until the silicon is exposed. The PR is removed using acetone and the wafer is placed in a 30% concentrated potassium hydroxide bath to etch the now exposed silicon in the microcavity features. The <100> face is etched while the <111> face prevents etching which creates an inverted pyramidal shape when the process is over. Next, a layer of PI2611 polyimide is spun over the wafer and cured. AZ5124 EIR PR is spun over the wafer and undergoes lithography again using the same mask as before aligned to match the features. However, the PR this time is used as a negative resist so that after developing with AZ400K 1:4, only the microcavity features are covered with PR. Then a nickel metal layer is deposited on top of the wafer using the Cooke E-beam Evaporator. The PR is removed during a

lift-off process using Microposit Remover 1165. With the microcavity features now exposed and the nickel serving as the mask, the wafer is etched in the Slave RIE from before using a mixture of CF_4 and O_2 as the etchant gases. The backside of the wafer must be etched with CF_4 to remove the silicon nitride layer from before. After the polyimide is fully removed from the cavities, the metal is patterned through lithography using AZ4620 as the PR and a mask designed to use the nickel as the device electrode. The nickel is etched using an etch solution comprised of water, nitric acid, and hydrochloric acid with a ratio of 4:1:5. A nickel etchant can be an alternative to the etch solution. After the nickel is etched, the AZ4620 PR is spun across the surface to protect the wafer during dicing. The wafer is cut into separate devices using the Disco DAD-6TM Wafer Dicing Saw. This process is illustrated in Figure 5.

A conductive silver epoxy is used to attach separate wires onto the nickel electrode and the silicon on the backside. After curing the silver epoxy the surface is then covered by Torr Seal epoxy as much as possible without covering the microcavity device. Some of the surface will still have nickel exposed. After curing the Torr Seal, the device is ready to be loaded into the chamber. When loading the device, the wires of the device and the feedthrough wires are soldered together. They are then covered by Kapton tape to reduce parasitic glow discharges.

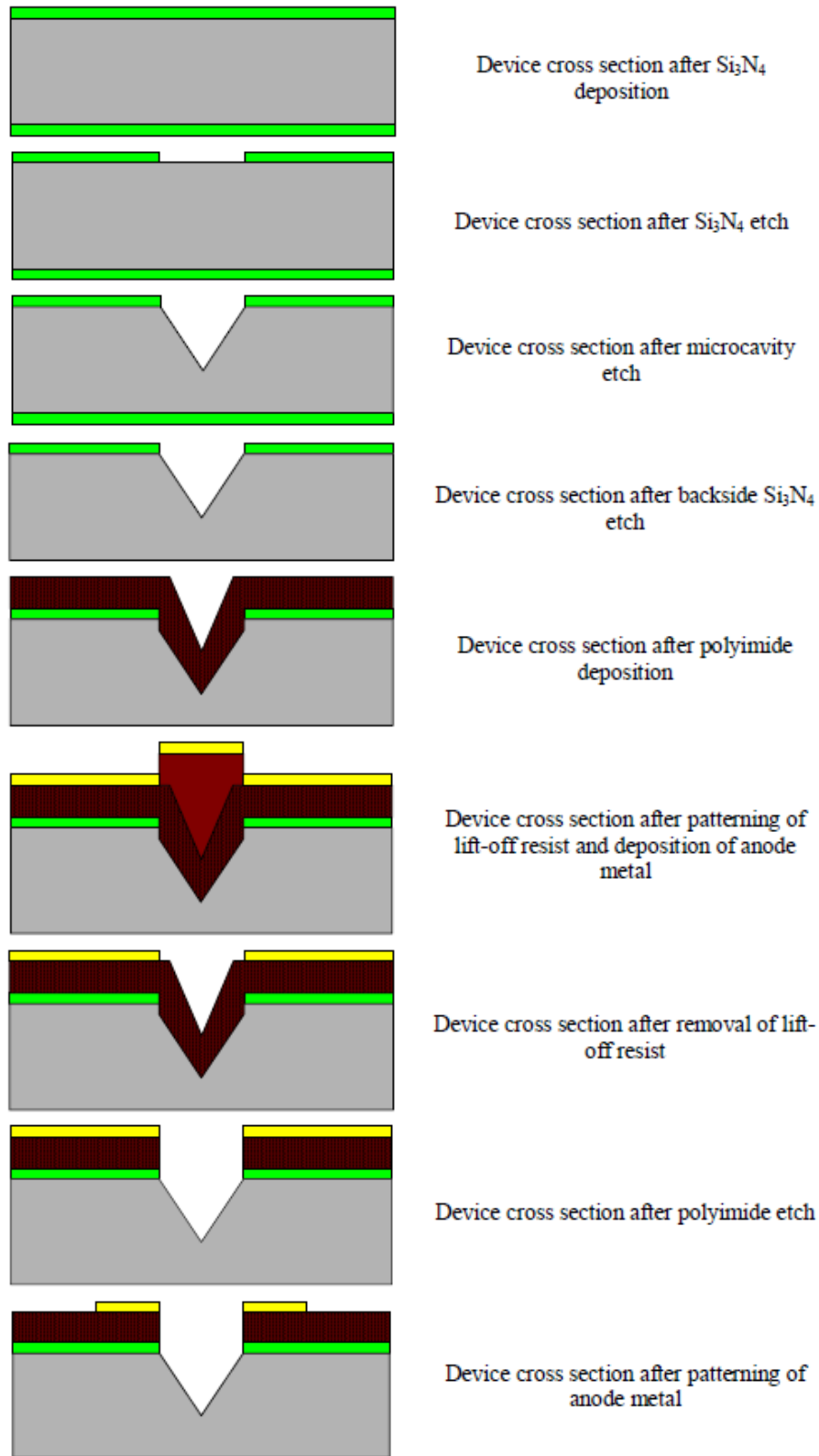


Figure 5. Cross-sectional diagram of the device structure at each stage of the fabrication process [4].

3.2 Experimental Setup

Figure 6 shows an external view of the chamber that was used to test the devices. There are two sets of vacuum wire feedthroughs that are used to connect external components to the inside of the chamber. The first set has two 20-gauge wires that connect AC power to the disc-shaped electrodes. The second set has twelve 12-gauge wires that connect any desired device within the chamber. The wires are insulated except at the tips.

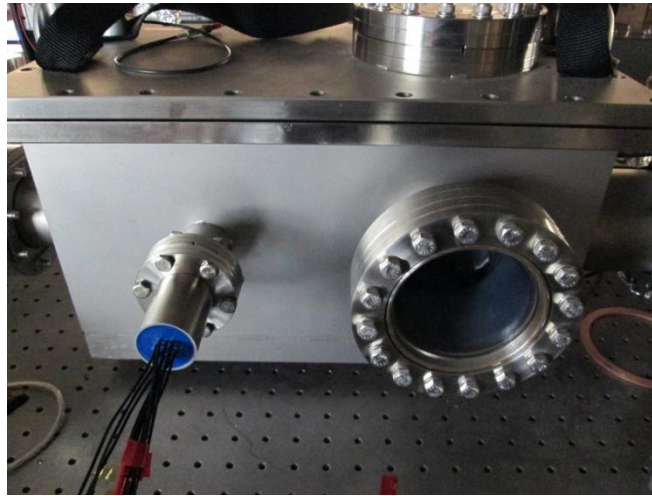


Figure 6. Photograph of the test chamber: viewing window on right and wire feedthrough on left.

The disc-shaped electrodes used to generate the plasma are made of alumina (Al_2O_3) through a process of anodization allowing aluminum to be converted into a dielectric layer. This is to protect the metal aluminum from ion bombardment by the plasma during operation. A hole is drilled into the sides of the electrodes to allow connection with the aluminum metal as seen in Figure 7. Figure 8 shows the actual product with Petri dishes covering the portion jutting out of the Teflon encasing.

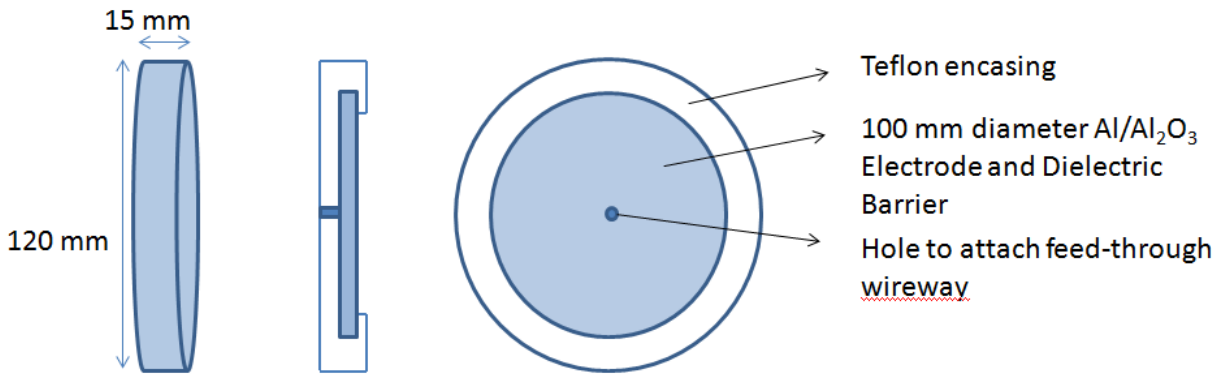


Figure 7. Diagram of disc-shaped electrodes.

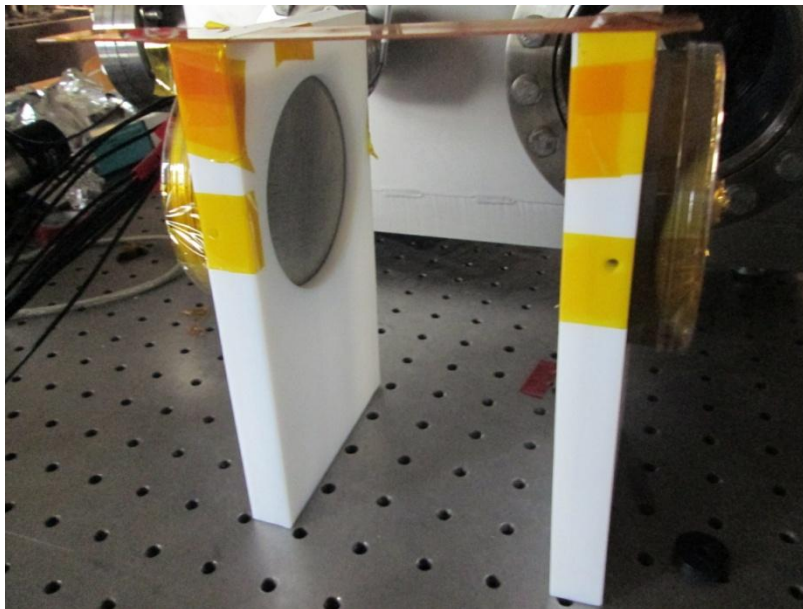


Figure 8. Teflon encasing with inserted disc-shaped electrodes covered by Petri dishes and Kapton tape.

A wafer holder was made by the Electrical and Computer Engineering (ECE) Shop at the University of Illinois at Urbana-Champaign. The holder could be placed in between the disc-shaped electrodes. The purpose for the wafer holder was to position devices at the same height depending on what kind of device was used. Wafer die could be loaded in the nine pockets, and wires would be connected from below so that all devices could be monitored at the same time. The holder is mainly made of Delrin, a type of plastic, with conductive components including a copper spring to allow wire contact with the devices. Figure 9 shows the diagram of the wafer

holder and Figure 10 shows the actual product designed by the ECE Shop, which had some modification.

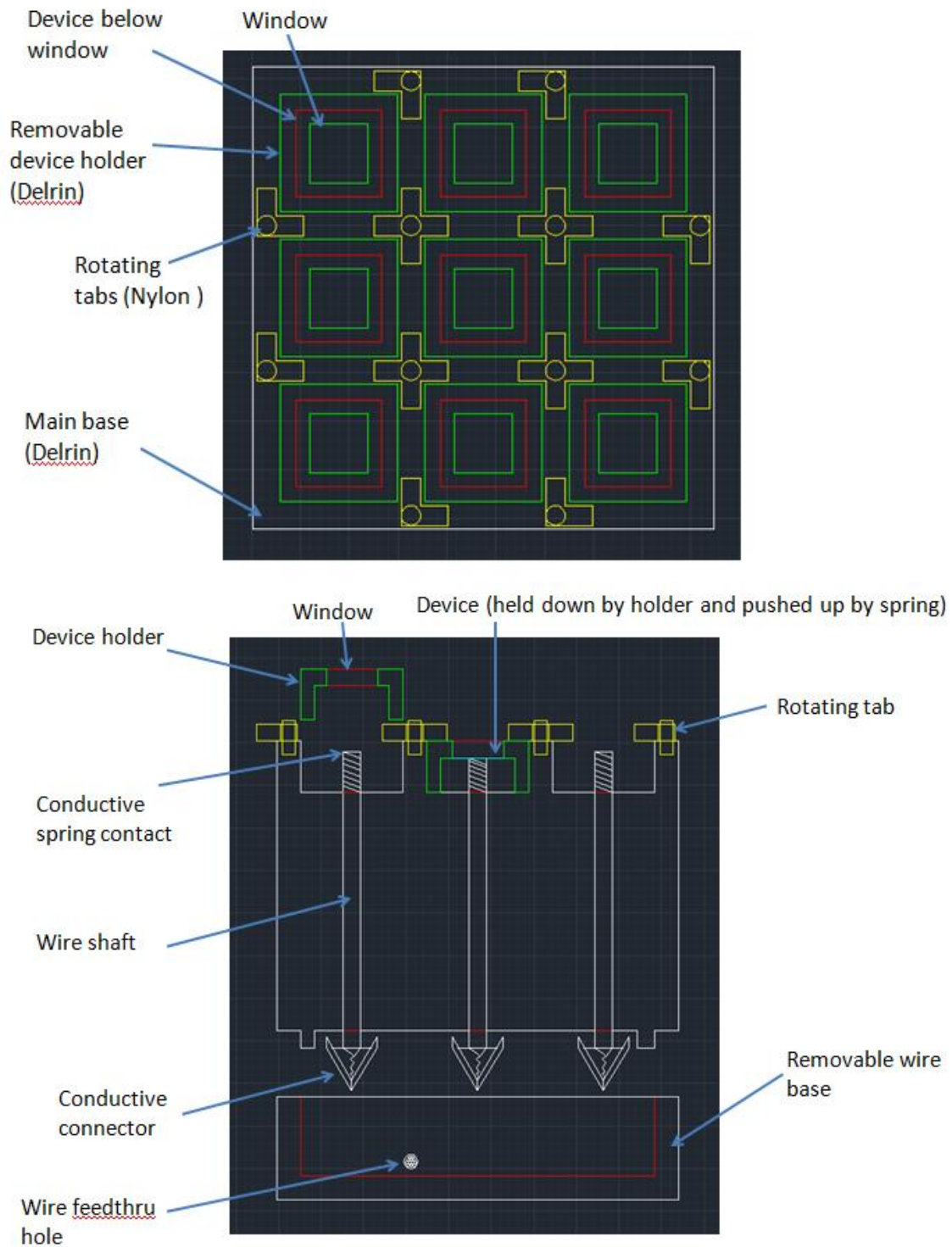


Figure 9. Design of the wafer holder.

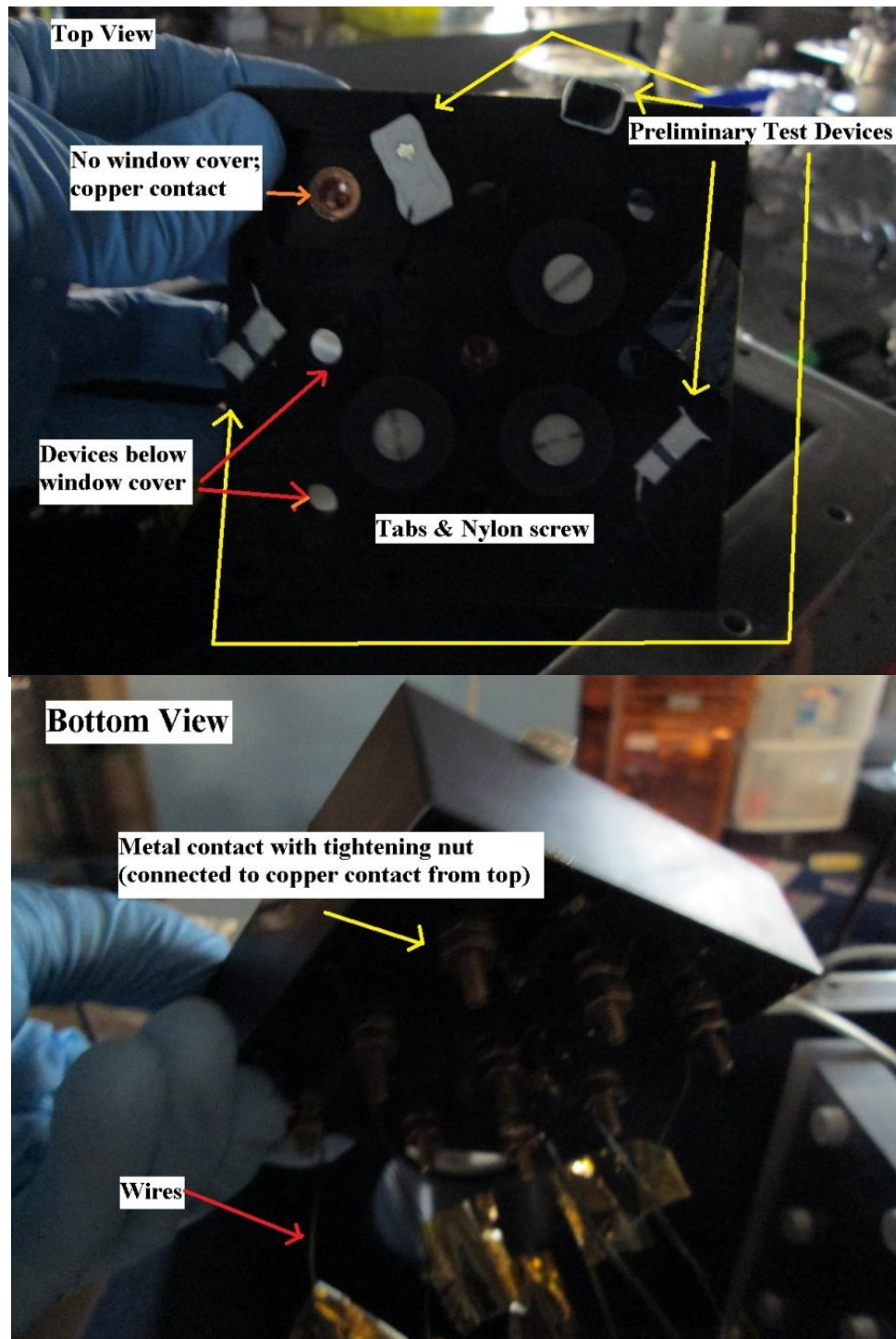


Figure 10. Wafer holder with different base portion than designed.

When pumping down the chamber, the roughing pump will evacuate the chamber to $\sim 10^{-3}$ Torr. The turbomolecular pump will then pump the system down further to around $\sim 10^{-6}$ Torr. The chamber is then filled with about 100 Torr neon and rough pumped back out to minimize other species of gas in the chamber. After minimizing the species of other gas, the chamber is filled again with ten Torr of neon gas. An AC sinusoid of more than 700 V at 20 kHz is driven across the disc-shaped electrodes to form the bulk plasma. Figure 11 shows an example of the apparatus in operation viewed through the chamber window of Figure 6. Figure 12 shows the connection diagram.

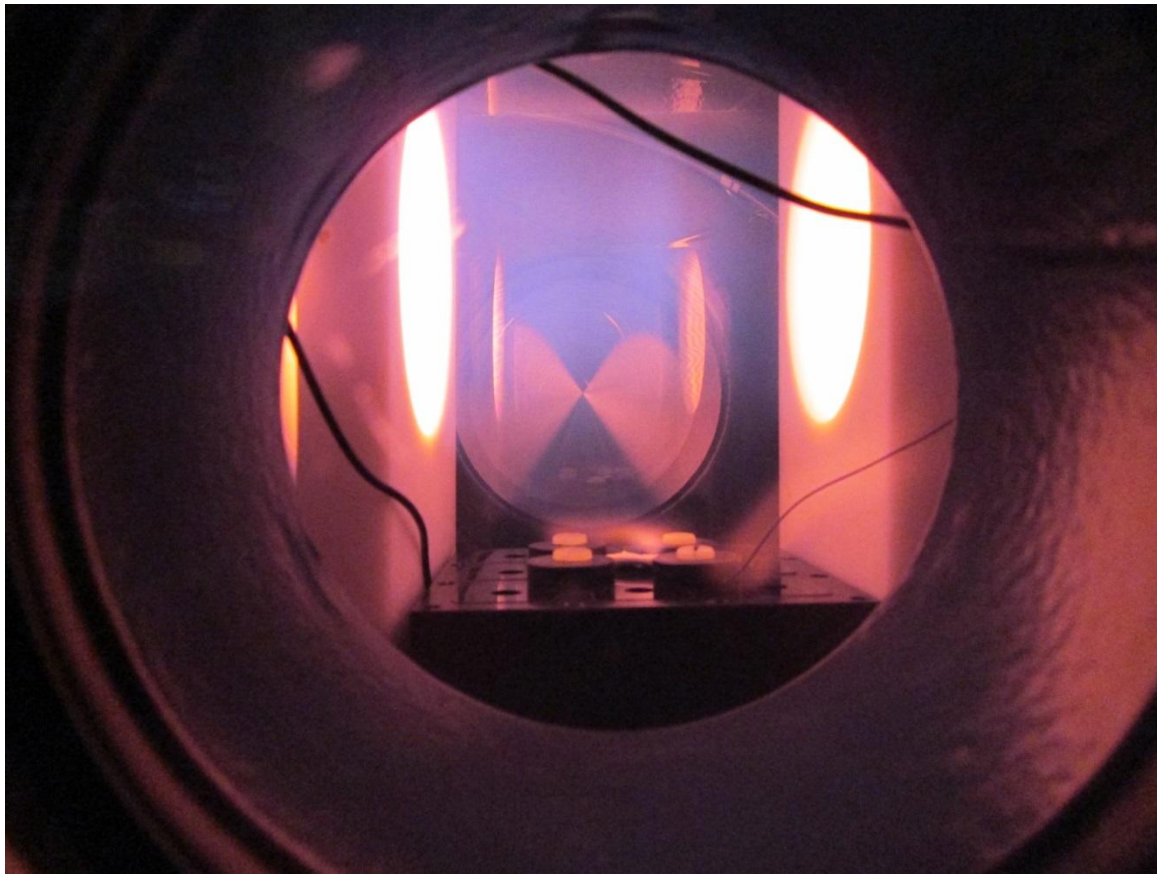


Figure 11. Photo taken during operation. Bulk plasma is formed between the two disc-shaped electrodes and the passive devices are loaded into the wafer holder below.

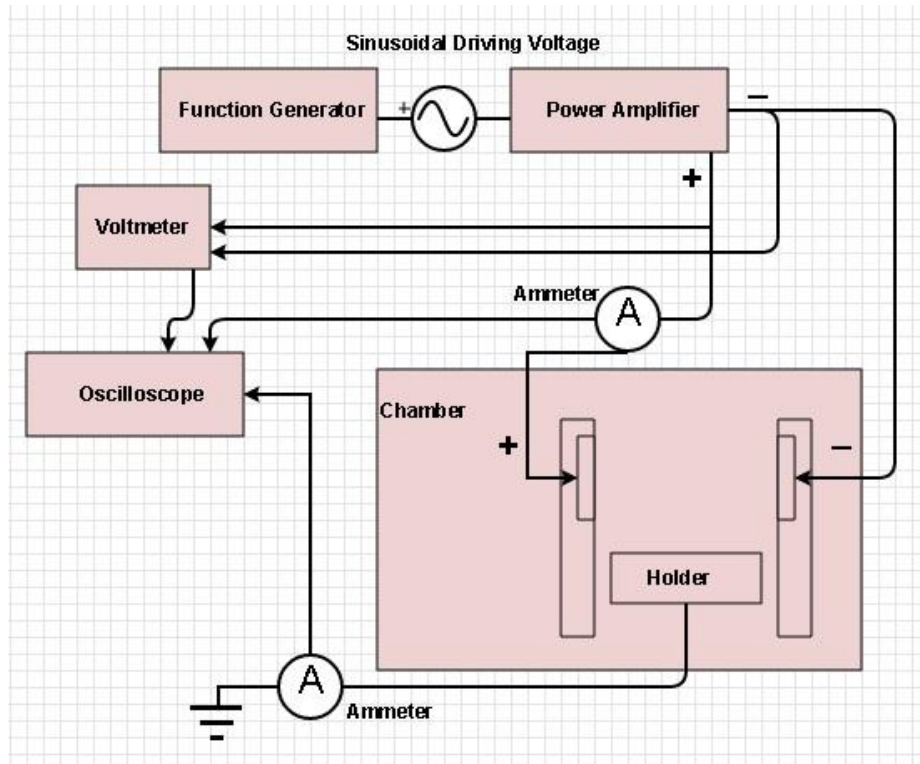


Figure 12: Electrical connection diagram.

Chapter 4. Results and Discussion

The photodetection signal from the Ni device was expected to be displayed as a significant spike in the current measurement, but that did not occur in this experiment. The previous device used in [4] and [5] was an active device where the plasma was first formed in the microcavity by biasing the metal anode (Ni) and the silicon cathode with an operating DC voltage of about 240 V with neon gas near atmospheric pressures. That operating context was changed tremendously in this experiment since the device was now being used as a passive device and the bulk plasma was generated using an AC voltage greater than 700 V in 10 Torr of neon gas.

The oscilloscope could only measure four components at a time. Channels 1 and 2 measured voltage and current across the disc-shaped electrodes made of aluminum and alumina. Channels 3 and 4 were swapped to measure different components in pairs. The first pair was a comparison between the standard device (Ni device) and the same type of device except with the nickel completely etched (no-Ni device) to determine if the nickel had any effect. The second pair was a comparison between the two no-Ni devices, one covered with a cover slip (covered device) and one without (uncovered device). The purpose of the cover slip was to keep the bulk plasma separate from the device to emphasize the signal based on photodetection. The last test was not a paired test, but it measured a single wire without any device attached to it to determine the effect of the plasma on a conductor. Figures 13-17 show the results.

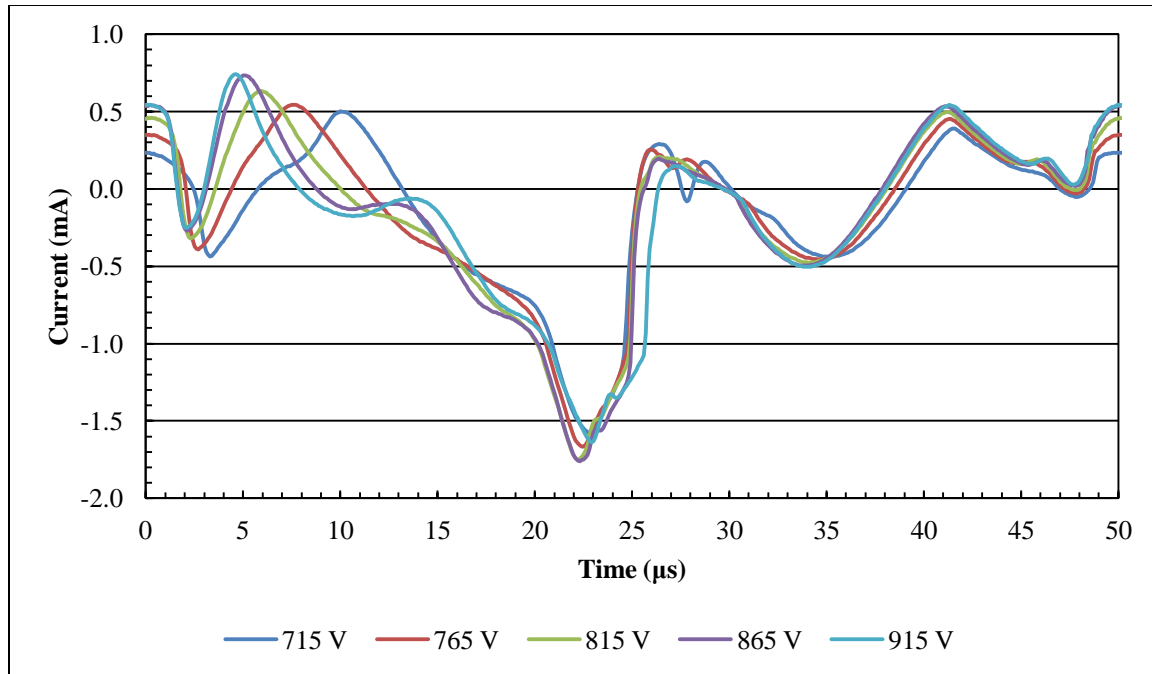


Figure 13: Oscilloscope of current measured through the Ni device for one period at different voltages.

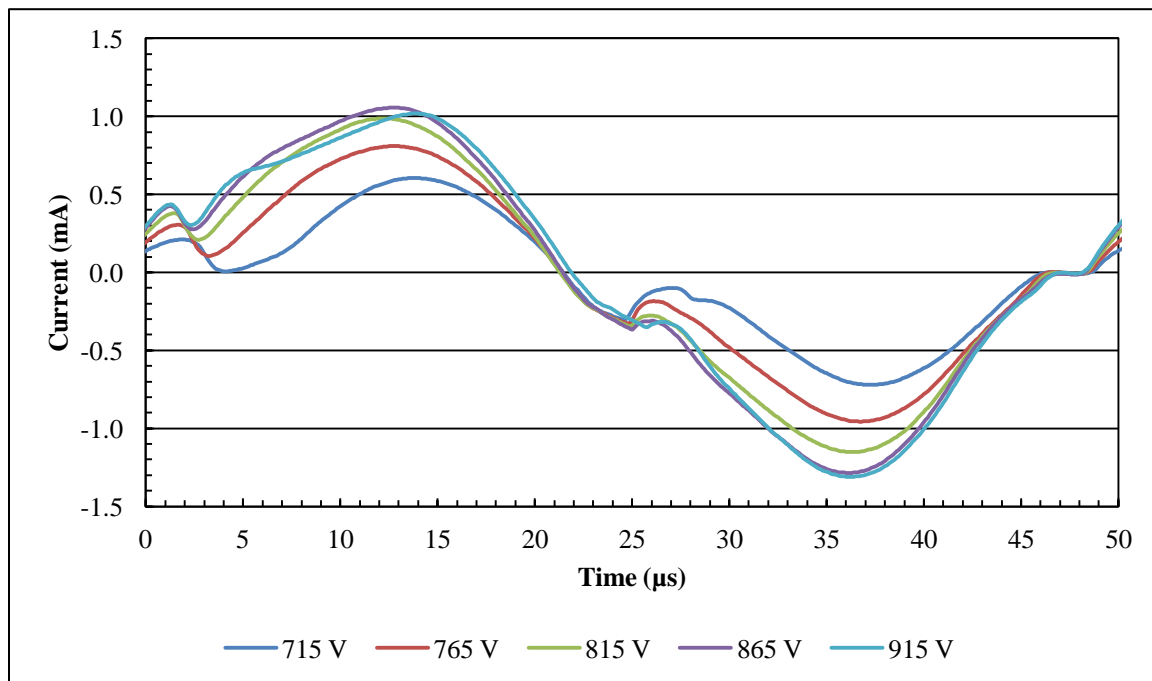


Figure 14: Oscilloscope of current measured through the no-Ni device for one period at different voltages.

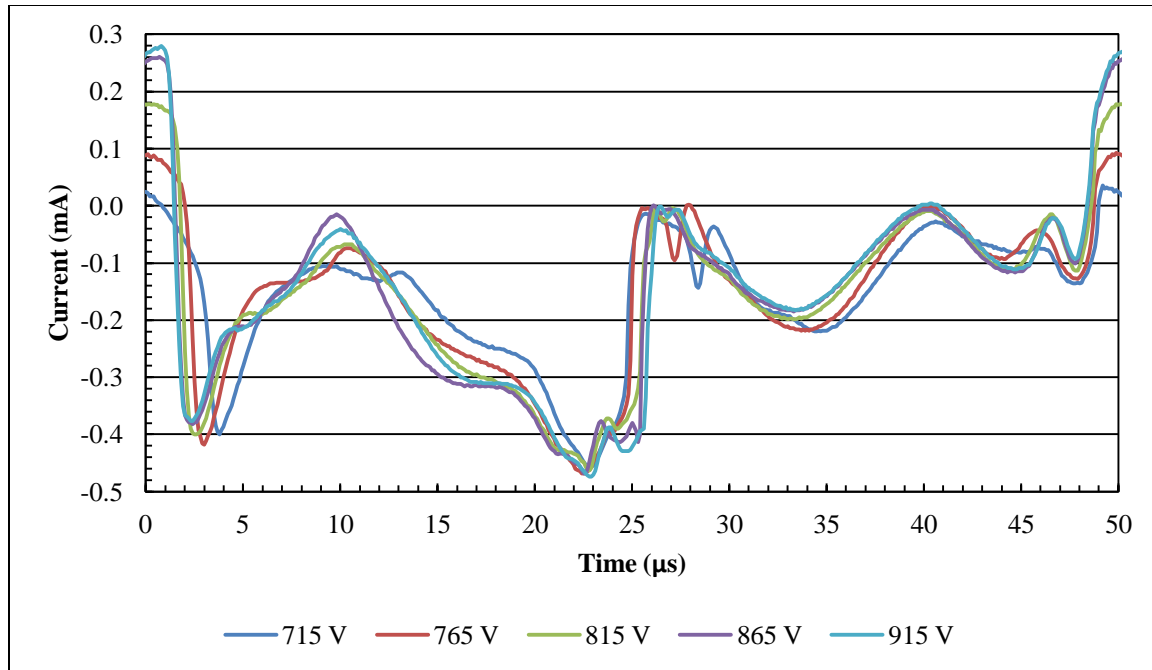


Figure 15: Oscillogram of current measured through the covered device for one period at different voltages.

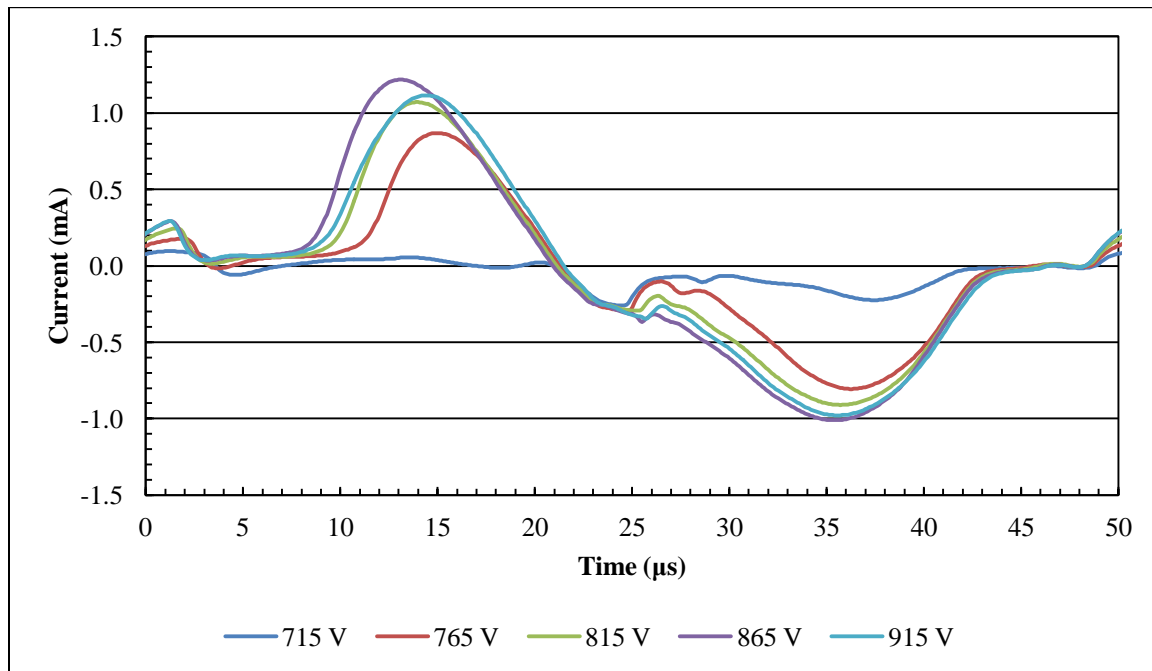


Figure 16: Oscillogram of current measured through the uncovered device for one period at different voltages.

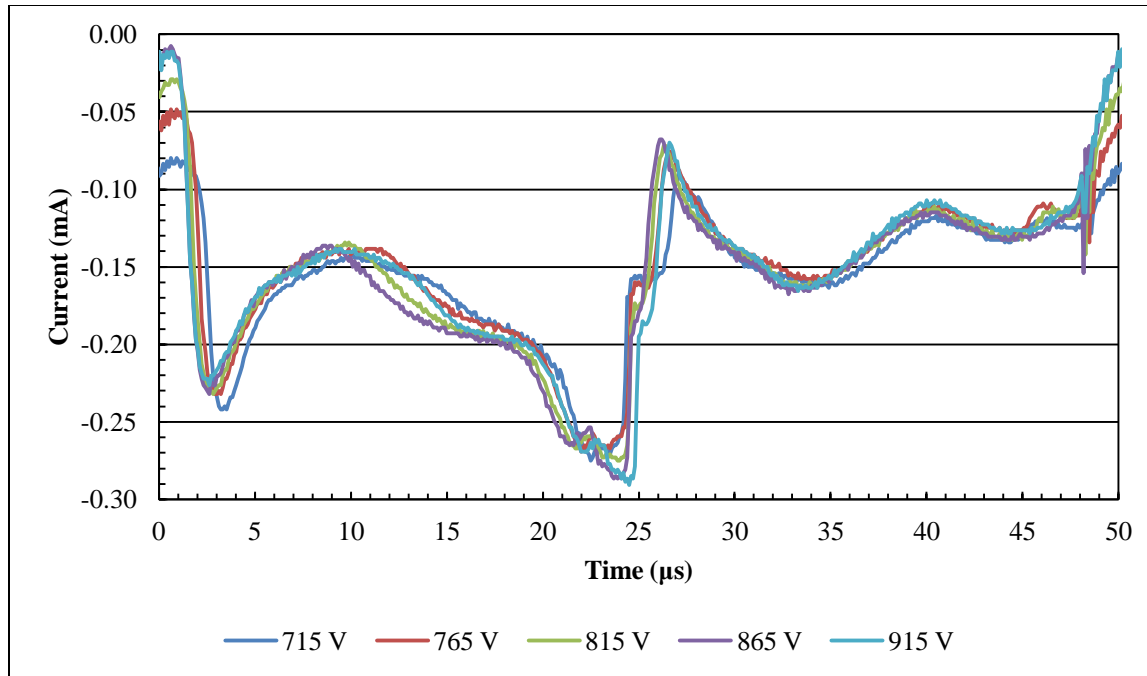


Figure 17: Oscillogram of current measured through the feedthrough wire for one period at different voltages.

Based on the initial results with raw data, it is clear that there is a difference between the Ni device and the no-Ni device. It is also clear that there is a difference between the covered device and the uncovered device. However, the shape of the graph for the Ni device and the covered device seems to be roughly the same for the wire data. In contrast, the graphs for the no-Ni device and the uncovered (no nickel) device are quite similar, which is to be expected.

As discussed earlier, the operating context of this experiment was different from the original operating conditions for the photodetector. As both the Ni device and the covered device seem to behave closer to a simple wire, it is difficult to tell whether photodetection is occurring. The no-Ni device, however, does not behave like a wire at all, and therefore, something else is happening in this case. It is clear from Figure 14 that the current is increasing as the voltage increases. The data seems to saturate at higher voltages beyond that range. Figure 18 shows the

integrated area under the curve of the first half cycle at increasing voltage and Figure 19 shows the second half cycle.

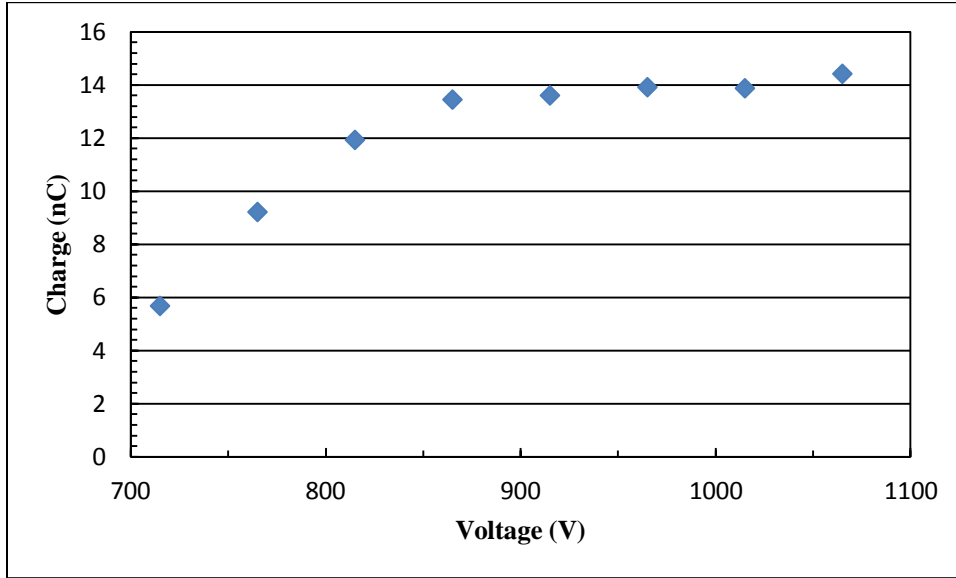


Figure 18: Integral of the current for the first half cycle for the no-Ni device.

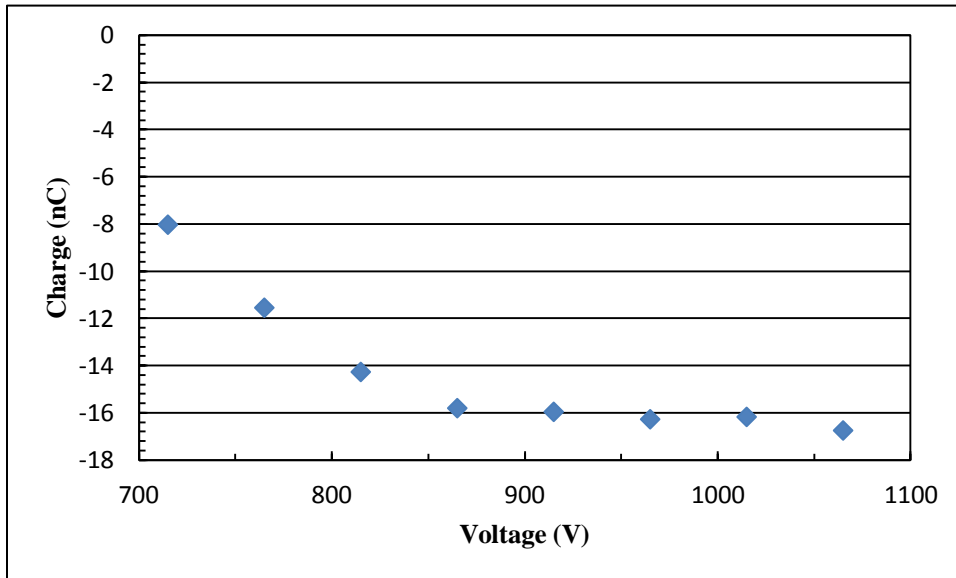


Figure 19: Integral of the current for the second half cycle for the no-Ni device.

It is important to note the linear region from about 715 V to 865 V. During operation, the intensity of the light of the bulk plasma increased with increasing voltage up to a certain point. Though this may not be the same type of photodetection mechanism mentioned in Section 2.3,

there may be a potential relationship between the intensity of the plasma and the current that would need further investigation to confirm.

Chapter 5. Limitations and Future Work

There were a couple experimental limitations that were identified when attempting to create the bulk plasma. The biggest issue was the test chamber as the chamber was made of metal. Uniform bulk plasma was hard to create because the driving voltage was an AC source with positive and negative polarity. Plasma would form in the area between the disc-shaped electrodes and the wall as the walls behaved as an electrical ground (see Figure 20, left). The electric field would be very strong in the area between the wall and the electrode due to the short distance between them. This electric field was much larger than the electric field between the two disc-shaped electrodes as the distance between the electrodes was many times greater than the electrode-wall distance. The test chamber was modified to reduce this wall interaction by filling the space between the wall and the electrode with a dielectric and also by varying the gas pressure until a desired bulk plasma was obtained. Another issue was that a glow discharge would form on the backside of the disc-shaped electrodes (see Figure 20, right). A Petri dish with the same diameter of the disc-shaped electrode was used as a cap to reduce this discharge from occurring.

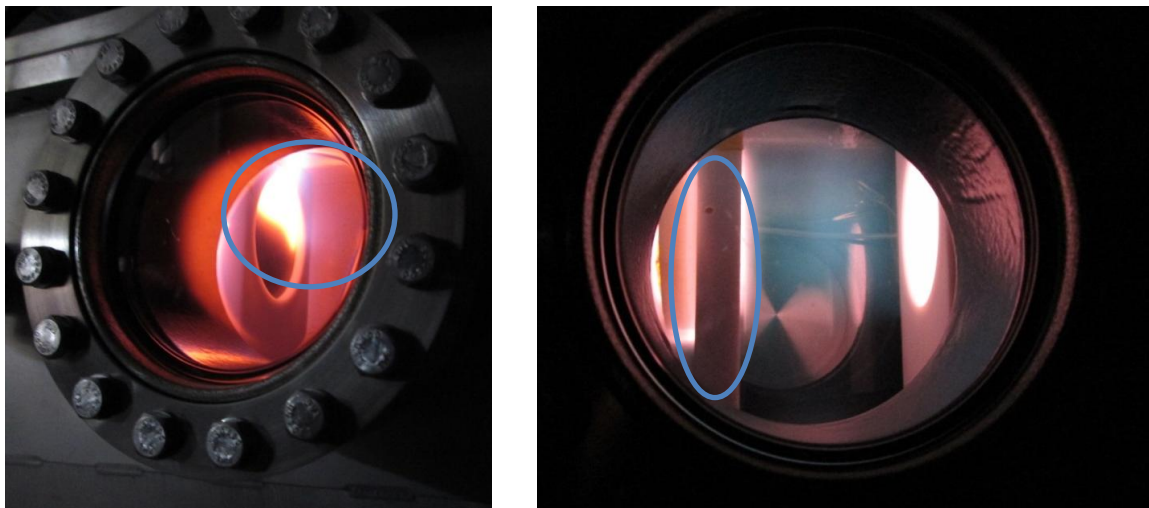


Figure 20: Example of the wall interaction (left) that affected the bulk plasma, and an example of glow discharge that formed on the backside of the electrode (right).

There are many suggestions for future work. First, the test environment needs to be redesigned to eliminate the issues mentioned above in creating the bulk plasma. Second, more experiments need to be designed in order to identify what is causing the device current to increase as the data seemed to indicate that the expected photodetection mechanism was not the source of increasing current. Third, a mapping of the device current at different locations on the xy-plane at different heights (z-direction) would be interesting to see how different positions affect the device current. Fourth, a relationship between the intensity of light, electron density, and device current needs to be ascertained in order to continue to pursue the idea of using this device as a diagnostic tool for semiconductor processing equipment.

References

- [1] S.-J. Park, J. Chen, C. J. Wagner, N. P. Ostrom, C. Liu, and J. G. Eden, "Microdischarge arrays: A new family of photonic devices," *IEEE Journal of Selected Topic in Quantum Electronics*, vol. 8, pp. 387-394, 2002.
- [2] K. H. Becker, K. H. Schoenbach, and J. G. Eden, "Microplasmas and applications," *J. Appl. Phys. D*, vol. 39, no. 11, p. R55, 2006.
- [3] S.-J. Park, J. G. Eden, and J. J. Ewing, "Photodetection in the visible, ultraviolet, and near-infrared with silicon microdischarge devices," *Applied Physics Letters*, vol. 81, no. 24, pp. 4529-4531, 2002.
- [4] N. P. Ostrom, "Photodetection in silicon pyramidal microdischarges," Ph.D. dissertation, University of Illinois at Urbana-Champaign, Urbana, IL, 2004.
- [5] N.P. Ostrom and J. G. Eden, "Microcavity plasma photodetectors: Photosensitivity, dynamic range, and the plasma-semiconductor interface," *Applied Physics Letters*, vol. 87, no. 14, 2005.
- [6] J. G. Eden and S.-J. Park, "Microcavity plasma devices and arrays: A new realm of plasma physics and photonic applications," *Plasma Physics and Controlled Fusion*, vol. 47, pp. B83-B92, 2005.
- [7] P. A. Tchertchian, "Hybrid plasma-semiconductor devices," Ph.D. dissertation, University of Illinois at Urbana-Champaign, Urbana, IL, 2010.
- [8] M. A. Lieberman and A. J. Lichtenberg, *Principles of Plasma Discharges and Materials Processing*, 2nd ed. New York, NY: Wiley, 2005.
- [9] B. Streetman and K. Sanjay, *Solid State Electronic Devices*, 6th ed. Upper Saddle River, NJ: Prentice Hall, 2005.
- [10] A. Fridman and L. A. Kennedy, *Plasma Physics and Engineering*, New York, NY: Taylor and Francis Books, Inc., 2004.